Southern Ocean oxygenation changes inferred from redox-sensitive trace metals across Marine Isotope Stage 11

E. E. Rohde[1], C. T. Hayes[1], N. Redmond[1], and S. K. Glassock[1]

[1] School of Ocean Science and Engineering, University of Southern Mississippi, Stennis Space Center, MS 39529, United States

Corresponding author: Christopher T. Hayes (christopher.t.hayes@usm.edu)

Key Points:

- Re, Mn and U behavior consistent with porewater oxygentation variation during MIS 11
- Mn, U and Re, respectively, are increasingly authigenic in ODP1094 sediments
- Potential for diagenetic effects such as remobilization of Re discussed

Abstract

Changes in the circulation of the Southern Ocean are known to have impacted global nutrient, heat, and carbon cycles during the glacial and interglacial periods of the late Pleistocene. Proxy-based records of these changes deserve continued scrutiny as the implications may be important for constraining future change. A record of authigenic uranium from the South Atlantic has been used to infer changes in deep-sea oxygenation and organic matter export over the past 0.5 million years. Since sedimentary uranium has the possible complication of remobilization, it is prudent to investigate the behavior of other redox-sensitive trace metals to confidently interpret temporal changes in oxygenation. Focusing here on the exceptionally long interglacial warm period, Marine Isotope Stage (MIS) 11, we found concurrent authigenic enrichments of uranium (U) and rhenium (Re) throughout MIS 12 to 10, overall supporting prior interpretations of low-oxygen periods. However, there are differential responses of Re and U to oxygen changes and some evidence of small-scale Re remobilization, which may involve differences in molecular-level reduction mechanisms. Peaks in authigenic manganese (Mn) intervening with peaks in Re and U indicate increases in porewater oxygenation which likely relate to increased Antarctic Bottom Water circulation at the onset of MIS11c and during the peak warmth of the interglacial around 400 ka.

1 Introduction

Analysis of ocean sediments can provide a window into past oceanic conditions and events. One particularly dynamic area in the world ocean is the Southern Ocean. In this region, the world's deep waters are upwelled to the surface as Circumpolar Deep Water and the world's densest bottom water is formed by downwelling Antarctic Bottom Water (AABW). Changes in the Southern Ocean circulation likely played a crucial role in glacial-interglacial air-sea carbon dioxide distribution, and therefore global climate, but the mechanisms involved are still being refined (Sigman et al., 2021). The reconstruction of deep-sea oxygenation by redox-sensitive trace metals in ocean sediments potentially provides an important constraint on the mechanisms of past climate change. This is because of dissolved oxygen's intimate relationship with deep ocean circulation (oxygen supply) and organic carbon flux (oxygen removal by respiration).

One particular sedimentary trace metal, uranium, becomes enriched in sediments with suboxic porewaters, as soluble porewater U(VI) is reduced to insoluble U(IV) and the porewater U gradient drives an enrichment of U sourced from bottom seawater into the sediments (Cochran & Krishnaswami, 1980; Klinkhammer & Palmer, 1991). This authigenic U has been used to infer past changes in organic carbon delivery to the sediments (Anderson et al., 1998; Chase et al., 2001; François et al., 1993; Kumar et al., 1995; Martınez-Garcia et al., 2009) or changes in bottom-water oxygenation relating to changes in ocean circulation (Costa et al., 2018; Hayes et al., 2014; Jaccard et al., 2009, 2016; Jacobel et al., 2020). This ascription of sedimentary uranium features to these past ocean conditions is non-trivial, however, as uranium can undergo "burn-down" or remobilization within a sediment core, especially during periods of changing oxygenation or reduced sedimentation rate (e.g., Frank et al., 2000; Mangini et al., 2001). Concomitant measurement of other metals whose redox sensitivity differs somewhat from uranium, therefore can help confirm whether observed authigenic features are primary emplacements or secondarily modified by changing redox fronts in the core (e.g., Crusius et al.,

1996; Crusius and Thomson, 2000; Nameroff et al., 2002; Rosenthal et al., 1995; Thompson et al., 1990).

In this study, we report manganese and rhenium concentrations at sub-millennial resolution from core ODP-1094 in the South Atlantic (53.2°S, 5.1°E, 2807 m water depth) to explore the fidelity of changes in oxygenation inferred from the previously reported authigenic uranium record (Glasscock et al., 2020). Marine Isotope Stage (MIS) 11 was a primary focus. This stage was identified as a unique interglacial over the past 0.5 million years, along with MIS5e (Hayes et al., 2014), to reveal a millennial-scale event during an interglacial period in which AABW circulation appears to have been reduced or slowed, possibly due to Antarctic ice melt (Glasscock et al., 2020). The MIS5e event involving Antarctic ice melt and reduction of AABW formation has been supported by several other proxies (Huang et al., 2020; Rohling et al., 2019), but the details of older periods are more uncertain. MIS11 is also an important climate period to study as an analogue to our present interglacial because this stage had similar orbital parameters (Droxler et al., 2003), global warmth of 0-2°C greater than pre-industrial and sea levels 6-13 m higher than present which likely involved significant loss of ice from Greenland and Antarctica (Candy et al., 2014; Dutton et al., 2015).

Similar to uranium, rhenium is soluble in oxidizing conditions but precipitates under suboxic conditions, close to or slightly later in the redox sequence than uranium does (Crusius et al., 1996; Crusius & Thomson, 2000). Thus, Re is expected to correlate with U in records not significantly influenced by post-emplacement diagenesis (e.g., Martınez-Garcia et al., 2009). Furthermore, in marine sediments rhenium has been found to have relatively greater authigenic enrichments over its lithogenic component compared to uranium and other trace metals (Colodner et al., 1993; Koide et al., 1986). This reduces uncertainty in correcting for the lithogenic component based on bulk measurements.

In contrast to uranium, manganese is preserved in solid oxides under oxidizing conditions. Authigenic manganese in some sedimentary settings can take the form of a carbonate (rhodochrosite), but this is generally limited to highly-organic laminated sediments (Neumann et al., 2002). While we have not specifically investigated the Mn mineralogy in core ODP-1094, our assumption in this pelagic setting that authigenic Mn takes the form of oxides. This authigenic Mn will be released into solution during diagenesis under suboxic conditions. Upon return to oxidizing conditions, the previously released dissolved Mn will be re-precipitated (Mangini et al., 2001). Therefore sedimentary authigenic Mn should anticorrelate with authigenic U (Jaccard et al., 2016) if the primary redox conditions of the surface sediments is faithfully recorded in the core. Coherent changes in all three metals (U, Re and Mn) would bolster the interpretation of syn-depositional oxygenation conditions inferred from the uranium record in core ODP-1094.

2 Materials and Methods

2.1 Sediment core material and age model

Sediment samples from Ocean Drilling Program Site 1094 were acquired from the Bremen Core Repository. This site is just south of the Antarctic Polar Front. The latest age model for this core (Fig. 1) has been developed by characterizing oxygen isotopes of benthic

foraminifera (Hasenfratz et al., 2019) tuned to the LR04 global benthic stack (Lisiecki & Raymo, 2005). The first 30,000 years of MIS11 are considered the substage MIS11c (Candy et al., 2014) which correspond to the peak warmth and atmospheric CO2 concentrations observed in Antarctic ice cores (Fig. 1). The shorter stadial MIS11b and interstadial MIS11a periods are not well-defined in the ODP-1094 benthic oxygen isotope record (Fig. 1), while there are firm tie points for the surrounding glacial periods MIS10 and 12. Notably, the independently datable speleothem records of the East Asian Monsoon (Cheng et al., 2016) place MIS11c (426 to 399 ka) in a timescale consistent with LR04.

Samples for the present study were selected at roughly 10 cm resolution to cover MIS11 (424 to 374 ka) as well as portions of the surrounding glacial periods MIS12 (450 to 424 ka) and MIS10 (374 to 369 ka) with an average temporal resolution of 0.7 ka. Throughout the section of the core studied here (71.5 to 55.5 meters composite depth, mcd), the average sedimentation rate is 17 cm/kyr. Samples from 55.5 to 69.3 mcd (369 to 440 ka) were all from Hole A of the Site and samples from 69.8 to 71.5 mcd (440 to 450 ka) were all from Hole D.

2.2 Redox-sensitive trace metal approach

Trace metals arrive in deep ocean sediments mainly through two processes. For one, trace metals are added to the sediments through in situ precipitation, called the authigenic phase. In contrast, trace metals are also deposited from mineral particles containing the trace elements substituted within mineral lattices, called the lithogenic phase (Morford & Emerson, 1999). Authigenic fractions of the measured metals in the present study were estimated here using the element thorium (Th), which due to its highly insoluble nature is assumed to be primarily found in lithogenic material in the ocean, with a minimal authigenic phase (Hayes et al., 2018). The authigenic phase of generic metal M (aM) can be defined as the measured metal minus an estimate of the lithogenic phase based on measured Th and the ratio of M to Th in lithogenic (lith) material (Eq. 1).

$$\boldsymbol{aM} = \boldsymbol{M} - \boldsymbol{Th} \times \left(\frac{\boldsymbol{M}}{\boldsymbol{Th}}\right)_{\boldsymbol{lith}} \qquad (1)$$

The U/Th ratio of lithogenic material is known to vary depending on the source of the lithogenic material, but is relatively well-characterized for the Atlantic sector of the Southern Ocean as 0.16 ± 0.03 g/g (Costa et al., 2020). This is about 40% lower than the U/Th ratio of the average upper continental crust (UCC) of 0.26 g/g (Rudnick & Gao, 2014). We have comparatively less information on the Mn/Th and Re/Th ratios of the lithogenic material within ODP-1094 sediments. Our first assumption is to use the Rudnick & Gao (2014) average UCC ratios of 1.9 x 10^{-5} g/g for Re/Th and 74 g/g for Mn/Th. As one estimate of the uncertainty in these ratios, another UCC assessment (Taylor & McLennan, 1995) estimated 3.7 x 10^{-5} g/g for Re/Th (nearly a factor of 2 higher than Rudnick & Gao, 2014) and 51 g/g for Mn/Th (about 30% lower than Rudnick & Gao, 2014). These ranges are considered in assessing uncertainty in the authigenic fraction determination.

The delivery of organic matter to the sediment-water interface is pertinent to this study because the respiration of this material plays a large role in setting porewater oxygen levels. Large changes in organic matter delivery can overprint any potential changes in deepwater oxygenation (e.g., Chase et al., 2001; François et al., 1993). To characterize changes in organic

matter delivery to the seafloor at ODP-1094, we utilize the barium to iron ratio (Ba/Fe) which has been reported at high resolution by X-Ray fluorescence (XRF) scanning throughout the length of the core (Jaccard et al., 2013). Biogenic barium, in the form of barite, is produced in the water column within microenvironments of sinking organic material (Dymond et al., 1992). The normalization to Fe attempts to account for dilution effects using the reference of relatively stable input of lithogenic Fe (Kumar et al., 1995) to qualitatively estimate the deposition rate of biogenic barium. The Ba/Fe ratio at this site was found to be well-correlated with three estimates of export production, namely ^{230}Th-normalized biogenic opal flux, total organic carbon flux and alkenone flux, over the past 150 ka (Jaccard et al., 2013).

We additionally measured concentrations of biogenic opal within the period of interest (MIS11) to help quantify the biogenic fraction of the sediments. Biogenic opal (hydrated, amorphous biogenic silica, SiO2·0.4H2O) was measured using a traditional alkaline leach spectrophotometric method (Mortlock & Froelich, 1989). For high opal sediments (<50% by weight), this method has a precision of ±4%. We also assessed the biogenic calcium carbonate content of the section of interest using the XRF-measured Ca/Fe ratio (Jaccard et al., 2013).

2.3 Sediment trace metal analysis

The sediments were prepared for inductively coupled plasma mass spectrometry (ICP-MS) analysis by weighing 50 mg of homogenized sediment into 22 mL Savillex beakers with a few milliliters of high-purity water. All reagents used in the following digestion were trace metal grade unless otherwise noted. Sediments were fully dissolved using 8 M nitric acid, heating to near dry at 150°C, and a series of alternating 1 mL additions and evaporation by heating of 26 M hydrofluoric acid and 9 M hydrogen peroxide. The alternating additions of hydrofluoric acid and hydrogen peroxide were repeated until the sample appeared fully dissolved when taken up in 0.5 ml 8 M nitric acid. Most samples received 2-3 rounds of this treatment. When fully dissolved the sample was dried down a final time at 150° C and then taken up in 2 ml of 2% optima grade nitric acid for ICP-MS analysis.

Trace element samples were dissolved in batches of 20 and analyzed in runs of 60-80 on an Element XR (Thermo Scientific) high-resolution ICPMS, using a PC-3 (Elemental Scientific) spray chamber for sample introduction. Concentrations of Mn, Re and Th were quantified using external standards and an internal indium standard to monitor matrix effects. Replicate sediment digestions were analyzed on roughly half of the samples and replicate concentrations agreed within 0.9% (Re), 1.1% (Th), and 2% (Mn). Procedural blanks corrections compared to measured signals averaged 12% (Re), 3% (Th) and 1% (Mn). Accuracy was assessed using USGS standards T207 and T211 for Re and Mn and SWS2010-1 (Anderson et al., 2012) for Th. Average and standard deviation of the measured standard concentrations (n = 7) were 6.91 ± 0.06 ng/g Re and 245 ± 2 μg/g Mn for T207, 6.23 ± 0.48 ng/g Re and 43.2 ± 1.5 μg/g Mn for T211, and 1.02 ± 0.07 ng/g Th for SWS2010-1. Concentrations of U were analyzed separately by isotope dilution as previously reported by Glasscock et al. (2020).

3 Results and Discussion

3.1 Bulk sediment composition

Biogenic opal concentrations ranged from about 90% by weight during the beginning of MIS11c to about 40% at the beginning of the glacial MIS10 (Fig. 2). Unfortunately, no samples from MIS12 were analyzed, but a very similar glacial-interglacial pattern in opal content from 40% in glacials to 90% in interglacials was found in ODP-1094 from MIS5 thru MIS1 (Jaccard et al., 2013) as well as for MIS8 to 7 (Janecek, 2001). This glacial-interglacial opal pattern was further found across all stages back to MIS12 for the lower resolution (average sedimentation rate 4 cm/kyr) core RC13-259 (Charles et al., 1991) which is roughly the same latitude and water depth as ODP-1094 but about 10 degrees longitude to the west (53.9°S, 4.9°W, 2677 m water depth).

Calcium carbonate content in ODP-1094 is generally low (<1%) except during peak interglacial conditions where CO2 outgassing from enhanced Southern Ocean upwelling during glacial terminations drove transient carbonate preservation events (Jaccard et al., 2013). This carbonate peak during MIS11c, as inferred from the Ca/Fe record, occurred from 403 to 396 ka on the current age model, coincident with a drop in opal content of about 20% (Fig. 2). Organic carbon content was <1.5% by weight over the last 150 ka in ODP-1094 and thus is not likely to significantly impact the content of the major sedimentary phases.

Outside of the carbonate preservation peaks then, the ODP-1094 sediments can be considered a mixture of biogenic opal and lithogenic material, which at this location is likely predominantly derived from ice-rafted detritus (IRD) (Kanfoush et al., 2002). Consistent with elevated IRD during glacial periods, thorium content is increased during MIS12 and 10 (Fig. 2). Furthermore, Th also increases and decreases, respectively across the stadial-interstadial substages of MIS11b and 11a, with mirroring changes in the measured opal content. Overall, this sediment composition analysis provides the expectation that lithogenic contributions to Re, Mn and U are likely to be especially low during interglacial MIS11c, where the biogenic fraction of the sediment is 90% or higher. In contrast, glacial and stadial stages may have more significant lithogenic components.

3.2 Lithogenic and authigenic metal fractions

An overview of the authigenic versus lithogenic content of the redox sensitive metals Re, Mn and U is given in Figure 3 in which the bulk concentrations are cross-plotted with measured Th concentrations. The assumed lithogenic ratios (Costa et al., 2020; Rudnick & Gao, 2014) are represented as a line on these plots and points falling above those lines indicate authigenic fraction of the redox-sensitive metal. Of the 3 metals, Re has the largest apparent authigenic component, as expected. The percentage contribution of lithogenic Re is a maximum of 2.5% which occurs at the beginning of MIS10 and is <1.5% for all of MIS11c and MIS12 (Fig. 4). Even using a factor of 2 higher lithogenic Re/Th ratio than assumed (Taylor & McLennan, 1995) would result in a small percentage correction on the measured Re.

Uranium is the next increasingly lithogenic of the metals, but with more consistent contrast between glacial stage lithogenic contribution of about 25% to <10% (and mostly <5%) lithogenic contributions within MIS11c (Fig. 4). The assumed uncertainty in the U/Th ratio of lithogenic material of about 20% also does not significantly affect authigenic U determination.

Mn is the most lithogenic studied here, with up to 60% lithogenic contribution during MIS12, 0-20% lithogenic contributions during MIS11c and 20-40% lithogenic contribution during MIS11b to MIS 10 (Fig. 4). Authigenic Mn determination is thus most sensitivite to uncertainty in the lithogenic Mn/Th ratio and there is a larger impact on the authigenic estimate in sections of the core with more lithogenic material. The available UCC estimates indicate that the Rudnick & Gao (2014) ratio (74 g/g) is larger than that (51 g/g) from Taylor & McLennan (1995). Thus, our estimates of aMn would be about 40% larger during MIS12, only about 5% larger during MIS11c, and about 15% larger during the remainder of MIS11 and 10 if the lower Mn/Th ratio were used. Because the peaks in aMn observed are much larger (factors of 2 to 5 above background, Fig. 5) than these relative differences, the uncertainty in lithogenic metal correction is still not likely to influence our interpretations of changes in authigenic enrichments in this core.

3.3. MIS12 to 10 redox record of ODP-1094

The concentrations of authigenic U, Re and Mn (aU, aRe, and aMn, respectively) are displayed versus age in figure 5, along with our proxy for organic matter delivery to the sediment (Ba/Fe). We highlight the 5 distinct periods of authigenic U enrichment observed across MIS12 to 11 observed by Glasscock et al. (2020). First, MIS12 was found to have significant aU enrichment, despite low local export production (yellow shading in Fig. 5). This must be due to a more poorly ventilated deep ocean during glacial periods, which is supported by several different proxy approaches (Anderson et al., 2019; Hoogakker et al., 2014; Jaccard et al., 2009, 2016; Jacobel et al., 2020; Wagner & Hendy, 2017). Low and constant aMn and highly enriched aRe in ODP-1094 during MIS12 are consistent with the view interpreted from U. The 15-30 ng/g (ppb) levels of enrichment of aRe is consistent with those found during MIS2 in core TN057-13 (same location as ODP-1094; Wagner & Hendy, 2017) and Cape Basin polar frontal zone core RC13-254 (48.6°S, 5.1°E, 3636 m water depth; Wagner & Hendry, 2017). This level of aRe enrichment is similar to that found in modern oxygen minimum zones and continental margin sedimentary environments, implying significant oxygen reduction in this area of the glacial deep ocean (Wagner et al., 2015; Wagner & Hendy, 2017).

Following the onset of MIS11, there are three periods of modest aU enrichment (~426 to 419 ka, 416 to 404 ka and 403 to 399 ka) that coincide with relatively high Ba/Fe levels (highlighted in orange in Fig. 5). These enrichments thus were ascribed to increased organic matter delivery and the associated porewater oxygen drawdown (Glasscock et al., 2020). It is possible that changes in deepwater oxygenation also played a role in these events, but it is difficult to disentangle this effect with the U data alone. Interestingly, aRe has a much greater contrast than aU between MIS12 and MIS11 enrichments. The MIS12 aU enrichment (2-3 ppm) is about twice as large as the more modest MIS11 aU peaks (~1-2 ppm), whereas the aRe enrichments during MIS12 (10-30 ppb) are 2-4 times larger than enrichments in MIS11 (2-10 ppb). Concentrations of aRe and aU throughout the 3 aU events between 400 and 426 ka are not significantly correlated on a sample-by-sample basis, which one might expect given the similar reduction potentials of the two elements. Nonetheless, the modest enrichments of aRe are grouped similarly to aU within these three sections. The Ba/Fe data suggest high and variable export production throughout these periods and thus the mis-match of aU and aRe on a sample-to-sample basis may represent small-scale remobilizations of Re, as the length scale of Re diffusion during reoxidation is expected to be greater than that of U (Crusius & Thomson, 2000). Furthermore, because authigenic metal accumulation happens at some depth below the sediment-water interface where our export production proxy has been recorded, there is reason to expect some offset in depth/time between the Ba/Fe record and both aU and aRe.We examine these possibilities further in the Section 3.4.

Notwithstanding some evidence of Re remobilization during early MIS 11, low aMn throughout the first 2 of the MIS11 aU events (425 ka to 404 ka; Fig. 5) indicate consistently low porewater oxygen levels. This is consistent with high organic matter input throughout this time and the respiration driven porewater oxygen drawdown appears to have more than compensated for a potentially more vigorous interglacial Southern Ocean circulation. Enhanced circulation is hinted at by the large aMn peak at the MIS12-11 transition, or Termination V. This aMn peak (centered at 432 ka) likely represents a large oxygenation event, coeval with precipitous drops in aU and aRe concentrations (Fig. 5). Rapid deep sea oxygenation at the end of the sluggish circulation of the prior glacial period may have been caused by increased Southern Ocean overturning, fueling the high MIS11 phytoplankton productivity at this site. This scenario, suggested to have been induced by poleward-shifted and/or strengthened Southern hemisphere westerly winds, appears to be common to all glacial terminations of the past million years (Anderson et al., 2009; Jaccard et al., 2013).

The third productivity-driven authigenic uranium/rhenium event at 402-399 ka coincided with a second large peak in aMn. This is not expected in terms of redox chemistry as there is evidence for both suboxic and oxygenated conditions. This period is coeval with peak biological productivity at ODP-1094, peak Antarctic warmth, peak atmospheric CO2 (Fig. 1) and the interglacial minimum in global ice volume (Elderfield et al., 2012). It is possible that the aMn formed just as local export flux was finally lessening after a long period of enhanced phytoplankton productivity, increasing porewater oxygen enough to form aMn and partially, but not fully, reoxidize previously emplaced aU and aRe. Thus it is difficult to distinguish whether this event represents increased Southern Ocean ventilation or a merely a significant reduction in organic matter delivery.

At the terminus of MIS11c, centered on 397 ka, an authigenic U peak appears with a strong decline of export flux (purple highlight in Fig. 5). Thus, Glasscock et al. (2020) ascribed this event to reduced oxygenation in the deep-sea and a possible reduction in AABW circulation. A significant and well-correlated peak in aRe and a strong decline in aMn at this time confirms the existence of suboxic porewaters likely due to reduced ventilation.

Moving toward the end stages of MIS11 and MIS 10 (390-370 ka), authigenic U gradually increases during low export productivity, suggesting a more gradual decline into a poorly ventilated glacial deep Southern Ocean (Fig. 5). There are less gradual and more abrupt increases in aRe during this time, consistent with the relatively large aRe emplacement during the prior glacial MIS12. Furthermore, a coherent aRe peak centered around 379 ka is surrounded by 2 single-point maxima in aMn. Since this all occurs with low export productivity, it is possible there were pulsed re-invigorations of AABW formation at these aMn peaks, as the overall shift to a weaker, glacial circulation scheme proceeded. These events in particular would be very difficult to discern from the aU data alone.

3.4 Feasibility of downcore Re diffusion

Given the evidence for at least partial remobilization of aRe during parts of MIS11c, we can explore the feasibility of the extent and magnitude of Re (and possible U) remobilization by examining the aRe/aU ratio of this section on the depth scale of the core (Fig. 5). In turbidite cores from the Madeira Abyssal Plain, Crusius & Thompson (2000) found that dissolved Re was apparently diffusing and re-precipitating in peaks 0.5 m to 3 m below the oxidation front in cores that had old authigenic metal enrichments exposed to oxygenated seawater under low (<1 cm/kyr) sedimentation rate conditions. In contrast, re-precipitated U in the Crusius and Thompson (2000) cores formed broader peaks and did not diffuse deeper than 0.5 m. The reason for the deeper length scale of Re re-precipitation after oxidative burndown is not clear. Re does have a larger molecular diffusion coefficient in seawater than U (5×10^{-6} cm/s^2 versus 2.5×10^{-6} cm/s^2) (Crusius et al., 1996; Li & Gregory, 1974), and dissolved Re may have a kinetically slower re-precipitation reaction than U (Crusius & Thomson, 2000). Because of the high average sedimentation rate of the ODP-1094 MIS10-12 section (~17 cm/kyr), we assume the 0.5 to 3 m re-precipitation length scales to be an upper limit on feasible length scales here.

The lowest aRe/aU ratios observed in the ODP-1094 section are around 5 mg/g which occur in MIS10 and MIS11a (58-60 mcd) (Fig. 6). Re and U are both conservative in the open ocean and the dissolved Re/U ratio is 2.7 mg/g (Colodner et al., 1993; Owens et al., 2011). The fact that aRe/aU ratios here (baseline of about 25-30 mg/g) are always higher than that found in seawater is evidence that there has been consistently greater aRe formation than aU formation throughout.

Moving on to the series of peaks in aRe/aU at much higher levels (50 to >200 mg/g), we evaluate these with respect to their relationship with the 5 aU enrichments described and the age-model based sedimentation rate (Fig. 6). While the average sedimentation rate in this section is relatively high (~17 cm/kyr), there is a brief period of about 8 kyr with a rate of 3 cm/kyr near the end of glacial aU enrichment during MIS12 (70.9 to 71.1 mcd). Interestingly, near and below this drop in sedimentation rate, there does not appear to be any large changes in the aRe/aU ratio that would suggest differential aRe diffusion (Fig. 6). There are large peaks in aRe/aU near the

beginning and end of the first of the three productivity-driven aU enrichments at 419-426 ka (67.8-69.8 mcd). The length scale of these peaks would be consistent with possible aRe remobilization, though they occur during a period of much higher sedimentation rate (34 cm/kyr). Thus, it does not seem likely that re-oxidation events during this period occurred due to reduced total sedimentation rate. Given the high and variable nature of the Ba/Fe productivity record the beginning of MIS11c (Fig. 5), we suggest that porewater oxygen levels could have remained fairly low but were variable due to pulsed inputs of organic matter export, either seasonally or on longer cycle timescales. We would suggest a similar argument for the series of aRe/aU peaks that occur during the second and third of the productivity driven aU peaks (62.1-63.8 mcd and 64.2-67.4 mcd) under even higher sedimentation rate (44 cm/kyr).

Finally, there is a relatively muted peak in aRe/aU during the late MIS11c aU enrichment purportedly (Glasscock et al., 2020) related to a reduction in Antarctic Bottom Water ventilation (395-398 ka, 60.4-61.4 mcd). This occurs within 0.5 m of a drop in sedimentation rate from 44 cm/kyr to 10 cm/kyr (Fig. 6), and thus could be related to Re re-precipitation. Nevertheless, Re and U continued to be buried at levels well-above their lithogenic background, and aMn remains low, in the period after this sedimentation rate drop (Fig. 5; 395-385 ka). This suggests there is no clear period of re-oxidation in the porewater to drive a complete "burndown". We suggest then that it may be subtle changes in the porewater redox conditions, that nonetheless remained suboxic, that could drive partial remobilization of aRe to a larger extent the aU. To resolve this issue, we suggest further study of porewater and sedimentary Re and U within suboxic sites. The Antarctic Polar Zone of the Atlantic, occupied by ODP-1094, appears to represent a uniquely transitional place in the contrast between oxic and suboxic sedimentary environments.

3.5 Implications for the paleo-interpretations of authigenic metal records

Despite some evidence for post-depositional Re movement, the major pattern of periods of enhanced suboxic porewater conditions are supported by both the aU and aRe proxies in the studied section of ODP-1094 (Fig. 5). However, it is clear that these 2 metals, while quite close in the redox spectrum, appear to have differing sensitivities, possibly related to the geochemical character of the sediments in different sections of the core. For instance, the ODP-1094 sediments have a strong compositional contrast between glacial and interglacial periods (Fig. 2) and changes in the major components of sediment and porewater could affect reduction reaction rates. The respective reduction reactions are believed to be ReO_4^- [Re(VII)] to ReO_2 (s) [Re(IV)] and $UO_2(CO_3)_3^{4-}$ [U(VI)] to UO_2 (s) [U(IV)] (Calvert & Pedersen, 1993), but these species are rarely directly observed and the reactions may be facilitated by unknown co-factors. Perhaps progress on this issue could be made from electrochemical sensors with marine sediments manipulated in the laboratory. Additionally investigating the mineralogy of the solid phase Mn (as an oxide or carbonate, for example) may be informative as this specific nature of this phase could also affect the redox condition of the sediments.

The utility of the additional information of aMn for paleoceanographic studies was also clear. While aU and aRe enrichments were out of phase for the most part as expected, the one exception was the ~401 ka event (Fig. 5) where it was difficult to discern balance between the competing effects of increased bottom water ventilation versus increased export production. It would be intriguing if geochemical modeling could recreate the oxidation/reduction potential (Eh) conditions necessary for the differential precipitation of this trio of metals through the types

of oxygenation changes likely seen in the ODP-1094 record. As far as paleoceanographic implications, it would of course be useful to observe evidence for these changes in other sectors of the Southern Ocean (e.g., Amsler et al., 2021) where similarly high sedimentation rate conditions exist.

4 Conclusions

This study focused on a climatically relevant past warm period, MIS11, with the motivation to scrutinize interpretations of past changes in Southern Ocean circulation based solely on an authigenic uranium record from core ODP-1094. We found concurrent authigenic enrichments of uranium and rhenium throughout MIS 12 to 10, overall supporting prior interpretations of low-oxygen periods. However, there are differential responses of Re and U to oxygen changes and some evidence of small-scale Re remobilization, which may involve differences in molecular-level reduction mechanisms. Peaks in authigenic manganese intervening with peaks in Re and U indicate increases in porewater oxygenation which likely relate to increased Antarctic Bottom Water circulation at the onset of MIS11c and during the peak warmth of the interglacial around 400 ka. We suggest future work ranging from investigating the molecular-level reduction mechanisms of Re and U under suboxic conditions to geochemical modeling of Eh conditions conducive to the observed trace metal patterns as well as corroborating the paleoceanographic conclusions derived here in other sectors of the Southern Ocean to the extent geophysical conditions allow.

Acknowledgments, Samples, and Data

This research was supported by the U.S. National Science Foundation (award 1658445) and the University of Southern Mississippi Eagle Scholars Program for Undergraduate Research. Melissa Gilbert is thanked for assistance with ICP-MS analysis. ODP samples used here were provided by the Bremen Core Repository. The U and Th data presented here are available at the NOAA Paleoclimatology database (https://www.ncdc.noaa.gov/paleo/study/28691). The Re, Mn, and opal data are available at Zenodo (https://doi.org/10.5281/zenodo.5071216).

Figure Captions

Figure 1. (Bottom to top) Age model for the section of ODP-1094 studied here based on benthic foraminiferal $\delta^{18}O$ (black points; ‰ with respect to Vienna Peedee Belemnite, Hasenfratz et al., 2019) compared with the Lisiecki & Raymo (2005) benthic stack (LR04) with Marine Isotope Stages (MIS) indicated (interstadials with gray background). The black triangles indicate the tie points between ODP-1094 and LR04 (Hasenfratz et al., 2019). The Ba/Fe ratio (green curve) is indicative of export productivity at this site (Jaccard et al., 2013). These deep sea records are compared with ice core records of Antarctic air temperature (Jouzel et al., 2007, blue curve) and atmospheric CO2 (Lüthi et al., 2008, red curve) on the AICC2012 timescale (Bazin et al., 2013).

Figure 2. Sedimentary composition of ODP-1094 between Marine Isotope Stages (MIS) 10 and 12, including (bottom to top), thorium (Th) concentration (black curve, this study), biogenic opal weight percentage (red curve, this study) and calcium carbonate content as inferred from the Ca/Fe ratio measured by X-Ray fluorescence (Jaccard et al., 2013). Error bars are ±4% for biogenic opal and are smaller than the symbol size for Th. Note there is a gap in data between about 400 and 403 ka in all three curves due to a core section break.

Figure 3. Bulk (measured) trace metal concentrations from ODP-1094 in sediments from Marine Isotope Stages 12 thru 10 (369 to 450 ka). The arrows indicate assumed ratios of lithogenic material for (A) Re/Th, (B) Mn/Th, and (C) U/Th. For a given Th concentration, concentrations above these lines are assumed to be authigenic phases. Error bars are smaller than symbol size. The blue arrows represent the ratios assumed in this study (that of Rudnick & Gao (2014) for Re and Mn, and Costa et al. (2020) for U) and the red arrows represent a secondary estimate (Taylor and McClennan (1995) for Mn and U) to illustrate the impact of uncertainty of this ratio on the determination of authigenic metals. The red arrow for Re (Taylor and McClennan, 1995) would not be visible below the blue arrow plotted.

Figure 4. Time-series of the authigenic (colored fill) and lithogenic (black fill) proportions of (bottom to top) bulk uranium, rhenium and manganese in the MIS12 to MIS12 section of ODP-1094 based on measured thorium and assumed metal/thorium ratios of lithogenic material. Note the rhenium plot is on a log-scale emphasizing low lithogenic contributions.

Figure 5. Sedimentary records from ODP-1094 (bottom to top) of authigenic uranium (aU, black curve; Glasscock et al., 2020), authigenic rhenium (aRe, blue curve, this study), authigenic manganese (aMn . orange curve, this study), and the Ba/Fe ratio (green curve x-ray fluorescence counts, Jaccard et al., 2013). Error bars in trace metal concentrations are smaller than symbols size. The periods highlighted with colored bars represent unique events in the oxygenation history, yellow reflecting glacial deoxygenation of deepwater, orange reflecting reduced porewater oxygen due to organic matter delivery to the sediments and purple representing a deoxygenation due to a possible interglacial reduction in deep ocean circulation. Note the break in the y-axis of the aRe panel and there is a core break noticeable in all curves between 403 and 400 ka. The location of age tie points are indicated by filled triangles at the top and boundaries of Marine Isotope Stages (MIS) are indicated.

Figure 6. Depth profile (in meters composite depth) from ODP-1094 of the ratio of authigenic rhenium to authigenic uranium (aRe/aU) in the bottom panel and the age-model-based sedimentation rate in the top panel. Note there are three points above the y-axis break at 200 mg/g on the aRe/aU panel. The location of age model tie points are indicated by the filled triangles at the top.

References

Amsler, H. E., Thöle, L. M., Stimac, I., Geibert, W., Ikehara, M., Kuhn, G., et al. (2021). Bottom water oxygenation changes in the Southwestern Indian Ocean as an indicator for enhanced respired carbon storage since the last glacial inception. *Climate of the Past Discussions*, 1–29. https://doi.org/10.5194/cp-2021-29

Anderson, R. F., Ali, S., Bradtmiller, L. I., Nielsen, S. H. H., Fleisher, M. Q., Anderson, B. E., & Burkle, L. H. (2009). Wind-driven upwelling in the Southern Ocean and the deglacial rise in atmospheric CO_2. *Science*, *323*, 1443–1448. https://doi.org/10.1126/science.1167441

Anderson, R. F., Fleisher, M. Q., Robinson, L. F., Edwards, R. L., Hoff, J. A., Bradley, S. B., et al. (2012). GEOTRACES intercalibration of 230Th, 232Th, 231Pa, and prospects for 10Be. *Limnology and Oceanography: Methods*, *10*, 179–213.

https://doi.org/10.4319/lom.2012.10.179

Anderson, R. F., Kumar, N., Mortlock, R. A., Froelilch, P. N., Kubik, P., Dittrich-Hannen, B., & Suter, M. (1998). Late-Quaternary changes in productivity of the Southern Ocean. *Journal of Marine Systems*, *17*, 497–514.

Anderson, R. F., Sachs, J. P., Fleisher, M. Q., Allen, K. A., Yu, J., Koutavas, A., & Jaccard, S. L. (2019). Deep-Sea Oxygen Depletion and Ocean Carbon Sequestration During the Last Ice Age. *Global Biogeochemical Cycles*, *33*(3), 301–317. https://doi.org/10.1029/2018GB006049

Bazin, L., Landais, A., Lemieux-Dudon, B., Toyé Mahamadou Kele, H., Veres, D., Parrenin, F., et al. (2013). An optimized multi-proxy, multi-site Antarctic ice and gas orbital chronology (AICC2012): 120-800 ka. *Climate of the Past*, *9*(4), 1715–1731. https://doi.org/10.5194/cp-9-1715-2013

Calvert, S. E., & Pedersen, T. F. (1993). Geochemistry of Recent oxic and anoxic marine sediments: Implications for the geological record. *Marine Geology*, *113*(1–2), 67–88. https://doi.org/10.1016/0025-3227(93)90150-T

Candy, I., Schreve, D. C., Sherriff, J., & Tye, G. J. (2014). Marine Isotope Stage 11 : Palaeoclimates, palaeoenvironments and its role as an analogue for the current interglacial. *Earth Science Reviews*, *128*, 18–51. https://doi.org/10.1016/j.earscirev.2013.09.006

Charles, D., Froelich, P. N., Mortlock, A., & Morley, J. (1991). Biogenic opal in Southern Ocean sediments over the last 450,000 years: implications for surface water chemistry and circulation. *Paleoceanography*, *6*(6), 697–728. https://doi.org/10.1029/91PA02477

Chase, Z., Anderson, R. F., & Fleisher, M. Q. (2001). Evidence from authigenic uranium for increased productivity of the glacial Subantarctic Ocean. *Paleoceanography*, *16*(5), 468–478. https://doi.org/10.1029/2000PA000542

Cheng, H., Edwards, R. L., Sinha, A., Spötl, C., Yi, L., Chen, S., et al. (2016). The Asian monsoon over the past 640,000 years and ice age terminations. *Nature*, *534*(7609), 640–646. https://doi.org/10.1038/nature18591

Cochran, J. K., & Krishnaswami, S. (1980). Radium, thorium, uranium and 210Pb in deep-sea sediments and sediment pore waters from the North Equatorial Pacific. *American Journal of Science*, *280*, 849–889. https://doi.org/10.2475/ajs.280.9.849

Colodner, D., Sachs, J., Ravizza, G., Turekian, K., Edmond, J., & Boyle, E. (1993). The geochemical cycle of rhenium: a reconnaissance. *Earth and Planetary Science Letters*, *117*, 205–221. https://doi.org/10.1016/0012-821X(93)90127-U

Costa, K. M., Anderson, R. F., McManus, J. F., Winckler, G., Middleton, J. L., & Langmuir, C. H. (2018). Trace element (Mn, Zn, Ni, V) and authigenic uranium (aU) geochemistry reveal sedimentary redox history on the Juan de Fuca Ridge, North Pacific Ocean. *Geochimica et Cosmochimica Acta*, *236*, 79–98. https://doi.org/10.1016/j.gca.2018.02.016

Costa, K. M., Hayes, C. T., Anderson, R. F., Pavia, F. J., Bausch, A., Deng, F., et al. (2020). ^{230}Th normalization: New insights on an essential tool for quantifying sedimentary fluxes in the modern and Quaternary ocean. *Paleoceanography and Paleoclimatology*, *35*(2), e2019PA003820. https://doi.org/10.1029/2019pa003820

Crusius, J., Calvert, S., Pedersen, T., & Sage, D. (1996). Rhenium and molybdenum in sediments as indicators of oxic, suboxic and sulfidic conditions of deposition. *Earth and Planetary Science Letters*, *145*, 65–78. https://doi.org/10.1016/S0012-821X(96)00204-X

Crusius, J., & Thomson, J. (2000). Comparative behavior of authigenic Re, U, and Mo during reoxidation and subsequent long-term burial in marine sediments. *Geochimica et Cosmochimica Acta*, *64*(13), 2233–2242. https://doi.org/10.1016/S0016-7037(99)00433-0

Droxler, A. W., Alley, R. B., Howard, W. R., Poore, R. Z., & Burckle, L. H. (2003). Unique and exceptionally long interglacial marine isotope stage 11: Window into earth warm future climate. In A. W. Droxler, R. Z. Poore, & L. H. Burkle (Eds.), *Earth's Climate and Orbital Eccentricity: The Marine Isotope Stage 11 Question* (Vol. 137, pp. 1–14). Washington, D. C.: American Geophysical Union. https://doi.org/10.1029/137GM01

Dutton, A., Carlson, A. E., Long, A. J., Milne, G. A., Clark, P. U., DeConto, R., et al. (2015). Sea-level rise due to polar ice-sheet mass loss during past warm periods. *Science*, *349*(6255), aaa4019. https://doi.org/10.1126/science.aaa4019

Dymond, J., Suess, E., & Lyle, M. (1992). Barium in deep-sea sediment: A geochemical proxy for paleoproductivity. *Paleoceanography*, *7*(2), 163–181. https://doi.org/10.1029/92PA00181

Elderfield, H., Ferretti, P., Greaves, M., Crowhurst, S., McCave, I. N., Hodell, D., & Piotrowski, A. M. (2012). Evolution of Ocean Temperature and Ice Volume Through the Mid-Pleistocene Climate Transition. *Science*, *337*, 704–709. https://doi.org/10.1126/science.1221294

François, R., Bacon, M. P., Altabet, M. A., & Labeyrie, L. D. (1993). Glacial/Interglacial changes in sediment rain rate in the SW Indian sector of subantarctic waters as recorded by ^{230}Th, ^{231}Pa, U and δ^{15}N. *Paleoceanography*, *8*(5), 611–629.

Frank, M., Gersonde, R., Rutgers van der Loeff, M., Bohrmann, G., Nurnberg, C. C., Kubik, P. W., et al. (2000). Similar glacial and interglacial export bioproductivity in the Atlantic sector of the Southern Ocean: Multiproxy evidence and implications for glacial atmospheric CO_2. *Paleoceanography*, *15*(6), 642–658. https://doi.org/10.1029/2000PA000497

Glasscock, S. K., Hayes, C. T., Redmond, N., & Rohde, E. (2020). Changes in Antarctic Bottom Water Formation During Interglacial Periods. *Paleoceanography and Paleoclimatology*, *35*, e2020PA003867. https://doi.org/10.1029/2020PA003867

Hasenfratz, A. P., Jaccard, S. L., Martínez-García, A., Sigman, D. M., Hodell, D. A., Vance, D., et al. (2019). The residence time of Southern Ocean surface waters and the 100,000-year ice age cycle. *Science*, *363*(6431), 1080–1084. https://doi.org/10.1126/science.aat7067

Hayes, C T, Anderson, R., Cheng, H., Conway, T. M., Edwards, R. L., Fleisher, M. Q., et al. (2018). Replacement Times of a Spectrum of Elements in the North Atlantic Based on Thorium Supply. *Global Biogeochemical Cycles*, *32*(9). https://doi.org/10.1029/2017GB005839

Hayes, Christopher T, Martínez-García, A., Hasenfratz, A. P., Jaccard, S. L., Hodell, D. A., Sigman, D. M., et al. (2014). A stagnation event in the deep South Atlantic during the last interglacial period. *Science*, *346*(6216), 1514–1517.

Hoogakker, B. A. A., Elderfield, H., Schmiedl, G., Mccave, I. N., & Rickaby, R. E. M. (2014). Glacial – interglacial changes in bottom-water oxygen content on the Portuguese margin. *Nature Geoscience*, *8*, 40–43. https://doi.org/10.1038/NGEO2317

Huang, H., Gutjahr, M., Eisenhauer, A., & Kuhn, G. (2020). No detectable Weddell Sea Antarctic Bottom Water export during the Last and Penultimate Glacial Maximum. *Nature Communications*, *11*(1), 1–10. https://doi.org/10.1038/s41467-020-14302-3

Jaccard, S. L., Galbraith, E. D., Martínez-García, A., & Anderson, R. F. (2016). Covariation of deep Southern Ocean oxygenation and atmospheric CO2 through the last ice age. *Nature*, *530*(7589), 207–210. https://doi.org/10.1038/nature16514

Jaccard, S. L., Hayes, C. T., Martínez-García, A., Hodell, D. A., Anderson, R. F., Sigman, D. M., & Haug, G. H. (2013). Two modes of change in Southern Ocean productivity over the past million years. *Science*, *339*(6126). https://doi.org/10.1126/science.1227545

Jaccard, S. L., Galbraith, E. D., Sigman, D. M., Haug, G. H., Francois, R., Pedersen, T. F., et al. (2009). Subarctic Pacific evidence for a glacial deepening of the oceanic respired carbon pool. *Earth and Planetary Science Letters*, *277*(1–2), 156–165. https://doi.org/10.1016/j.epsl.2008.10.017

Jacobel, A. W., Anderson, R. F., Jaccard, S. L., McManus, J. F., Pavia, F. J., & Winckler, G. (2020). Deep Pacific storage of respired carbon during the last ice age: Perspectives from bottom water oxygen reconstructions. *Quaternary Science Reviews*, *230*, 106065. https://doi.org/10.1016/j.quascirev.2019.106065

Janecek, T. R. (2001). Data report: Late Pleistocene biogenic opal data for Leg 177 Sites 1093 and 1094. In R. Gersonde, D. A. Hodell, & P. Blum (Eds.), *Proceedings of the Ocean Drilling Program, Scientific Results* (Vol. 177, pp. 1–5). Retrieved from http://www-odp.tamu.edu/publications/177_SR/chap_02/chap_02.htm

Jouzel, J., Masson-Delmotte, V., Cattani, O., Dreyfus, G., Falourd, S., Hoffman, G., et al. (2007). Orbital and millennial Antarctic climate variability over the past 800,000 years. *Science*, *317*, 793–796. https://doi.org/10.1126/science.1141038

Kanfoush, S. L., Hodell, D. A., Charles, C. D., Janecek, T. R., & Rack, F. R. (2002). Comparison of ice-rafted debris and physical properties in ODP Site 1094 (South Atlantic) with the Vostok ice core over the last four climatic cycles. *Palaeogeography, Palaeoclimatology, Palaeoecology*, *182*, 329–349. https://doi.org/10.1016/S0031-0182(01)00502-8

Klinkhammer, G. P., & Palmer, M. R. (1991). Uranium in the oceans: Where it goes and why. *Geochimica et Cosmochimica Acta*, *55*(7), 1799–1806. https://doi.org/10.1016/0016-7037(91)90024-Y

Koide, M., Hodge, V., Kay, P., Stallard, M., & Goldberg, E. D. (1986). Some comparative marine chemistries of platinum and iridium. *Applied Geochemistry*, *1*(2), 227–232. https://doi.org/10.1016/0883-2927(86)90006-5

Kumar, N., Anderson, R. F., Mortlock, R. A., Froelich, P. N., Kubik, P., Dittrich-Hannen, B., & Suter, M. (1995). Increased biological productivity and export production in the glacial Southern Ocean. *Nature*, *378*, 675–680. https://doi.org/10.1038/378675a0

Li, Y.-H., & Gregory, S. (1974). Diffusion of ions in seawater and in deep-sea sediments.

Geochimica et Cosmochimica Acta, *38*(5), 703–734. https://doi.org/10.1016/0016-7037(74)90145-8

Lisiecki, L. E., & Raymo, M. E. (2005). A Pliocene-Pleistocene stack of 57 globally distributed benthic δ 18O records. *Paleoceanography*, *20*(1), 1–17. https://doi.org/10.1029/2004PA001071

Lüthi, D., Le Floch, M., Bereiter, B., Blunier, T., Barnola, J.-M., Siegenthaler, U., et al. (2008). High-resolution carbon dioxide concentration record 650,000-800,000 years before present. *Nature*, *453*, 379–382. https://doi.org/10.1038/nature06949

Mangini, A., Jung, M., & Laukenmann, S. (2001). What do we learn from peaks of uranium and of manganese in deep sea sediments? *Marine Geology*, *177*(1–2), 63–78. https://doi.org/10.1016/S0025-3227(01)00124-4

Martınez-Garcia, A., Rosell-Mele, A., Geibert, W., & Gersonde, R. (2009). Links between iron supply, marine productivity, sea surface temperature, and CO_2 over the last 1.1 Ma. *Paleoceanography*, *24*, 1–14. https://doi.org/10.1029/2008PA001657

Morford, J. L., & Emerson, S. (1999). The geochemistry of redox sensitive trace metals in sediments. *Geochimica et Cosmochimica Acta*. https://doi.org/10.1016/S0016-7037(99)00126-X

Mortlock, R. A., & Froelich, P. N. (1989). A simple method for the rapid determination of biogenic opal in pelagic marine sediments. *Deep-Sea Research Part A, Oceanographic Research Papers*, *36*(9), 1415–1426. https://doi.org/10.1016/0198-0149(89)90092-7

Nameroff, T. J., Balistrieri, L. S., & Murray, J. W. (2002). Suboxic trace metal geochemistry in the eastern tropical North Pacific. *Geochimica et Cosmochimica Acta*, *66*(7), 1139–1158. https://doi.org/10.1016/S0016-7037(01)00843-2

Neumann, T., Heiser, U., Leosson, M. A., & Kersten, M. (2002). Early diagenetic processes during Mn-carbonate formation: Evidence from the isotopic composition of authigenic Ca-rhodochrosites of the Baltic Sea. *Geochimica et Cosmochimica Acta*, *66*(5), 867–879. https://doi.org/10.1016/S0016-7037(01)00819-5

Owens, S. A., Buesseler, K. O., & Sims, K. W. W. (2011). Re-evaluating the ^{238}U-salinity relationship in seawater: Implications for the ^{238}U-^{234}Th disequilibrium method. *Marine Chemistry*, *127*(1–4), 31–39. https://doi.org/10.1016/j.marchem.2011.07.005

Rohling, E. J., Hibbert, F. D., Grant, K. M., Galaasen, E. V., Irvalı, N., Kleiven, H. F., et al. (2019). Asynchronous Antarctic and Greenland ice-volume contributions to the last interglacial sea-level highstand. *Nature Communications*, *10*(1). https://doi.org/10.1038/s41467-019-12874-3

Rosenthal, Y., Lam, P., Boyle, E. A., & Thomson, J. (1995). Authigenic cadmium enrichments in suboxic sediments: precipitation and postdepositional mobility. *Earth and Planetary Science Letters*, *132*(1–4), 99–111. https://doi.org/10.1016/0012-821X(95)00056-I

Rudnick, R. L., & Gao, S. (2014). Composition of the Continental Crust. In H. D. Holland & K. K. Turekian (Eds.), *Treatise on Geochemistry (Second Edition)* (Vol. 4, pp. 1–51). Oxford, UK, doi: 10.1016/B978-0-08-095975-7.00301-6: Elsevier. https://doi.org/10.1016/B978-0-08-095975-7.00301-6

Sigman, D. M., Fripiat, F., Studer, A. S., Kemeny, P. C., Martínez-García, A., Hain, M. P., et al. (2021). The Southern Ocean during the ice ages: A review of the Antarctic surface isolation hypothesis, with comparison to the North Pacific. *Quaternary Science Reviews, 254*. https://doi.org/10.1016/j.quascirev.2020.106732

Taylor, S. R., & McLennan, S. M. (1995). The geochemical evolution of the continental crust. *Reviews of Geophysics, 33*(2), 241–265. https://doi.org/10.1029/95RG00262

Thompson, J., Wallace, H. E., Colley, S., & Toole, J. (1990). Authigenic uranium in Atlantic sediments of the last glacial stage - a diagenetic phenomenon. *Earth and Planetary Science Letters, 98*, 222–232. https://doi.org/10.1016/0012-821X(90)90061-2

Wagner, M., & Hendy, I. L. (2017). Trace metal evidence for a poorly ventilated glacial Southern Ocean. *Quaternary Science Reviews*, *170*, 109–120. https://doi.org/10.1016/j.quascirev.2017.06.014

Wagner, M., Hendy, I. L., McKay, J. L., & Pedersen, T. F. (2015). Redox chemistry of West Antarctic Peninsula margin surface sediments. *Chemical Geology*, *417*, 102–114. https://doi.org/10.1016/j.chemgeo.2015.10.002

Figure 1.

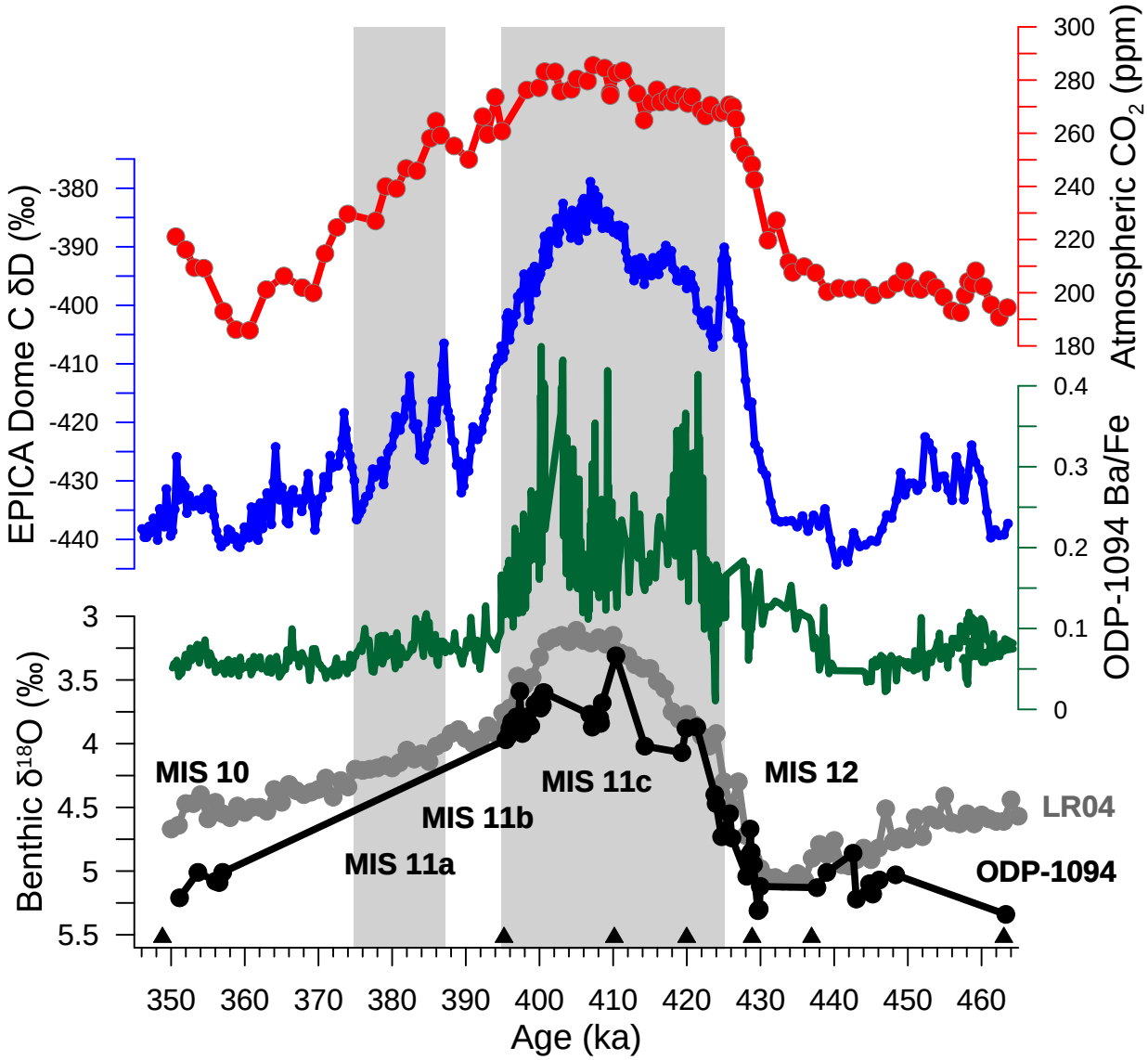
EPICA Dome C δD (‰)
-380
-390
-400
-410
-420
-430
-440
Atmospheric CO2 (ppm)
300
280
260
240
220
200
180
ODP-1094 Ba/Fe
0.4
0.3
0.2
0.1
0
Benthic δ18O (‰)
3
3.5
4
4.5
5
5.5
MIS 10
MIS 11a
MIS 11b
MIS 11c
MIS 12
LR04
ODP-1094
350
360
370
380
390
400
410
420
430
440
450
460
Age (ka)

Figure 2.

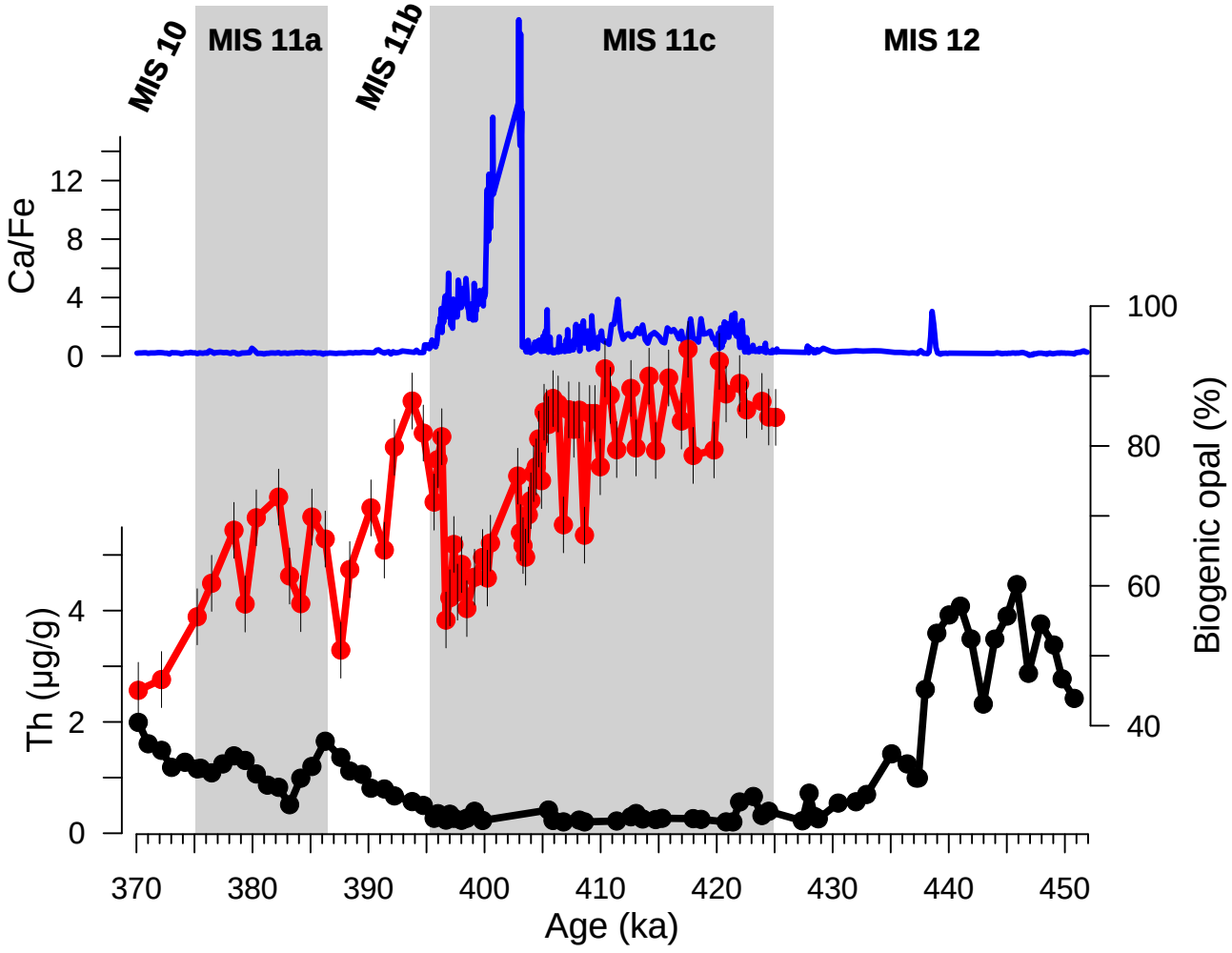
MIS 10
MIS 11a
MIS 11b
MIS 11c
MIS 12
Ca/Fe
0
4
8
12
Th (µg/g)
0
2
4
Biogenic opal (%)
40
60
80
100
370
380
390
400
410
420
430
440
450
Age (ka)

Figure 3.

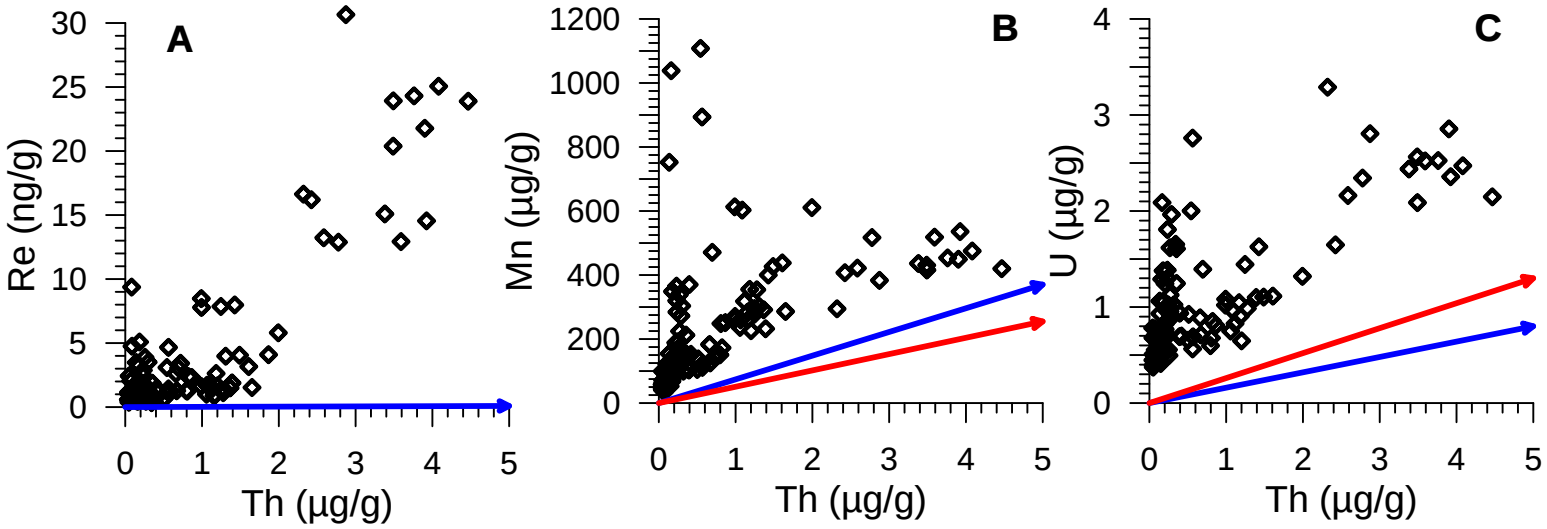
A
Re (ng/g)
Th (µg/g)
B
Mn (µg/g)
Th (µg/g)
C
U (µg/g)
Th (µg/g)

Figure 4.

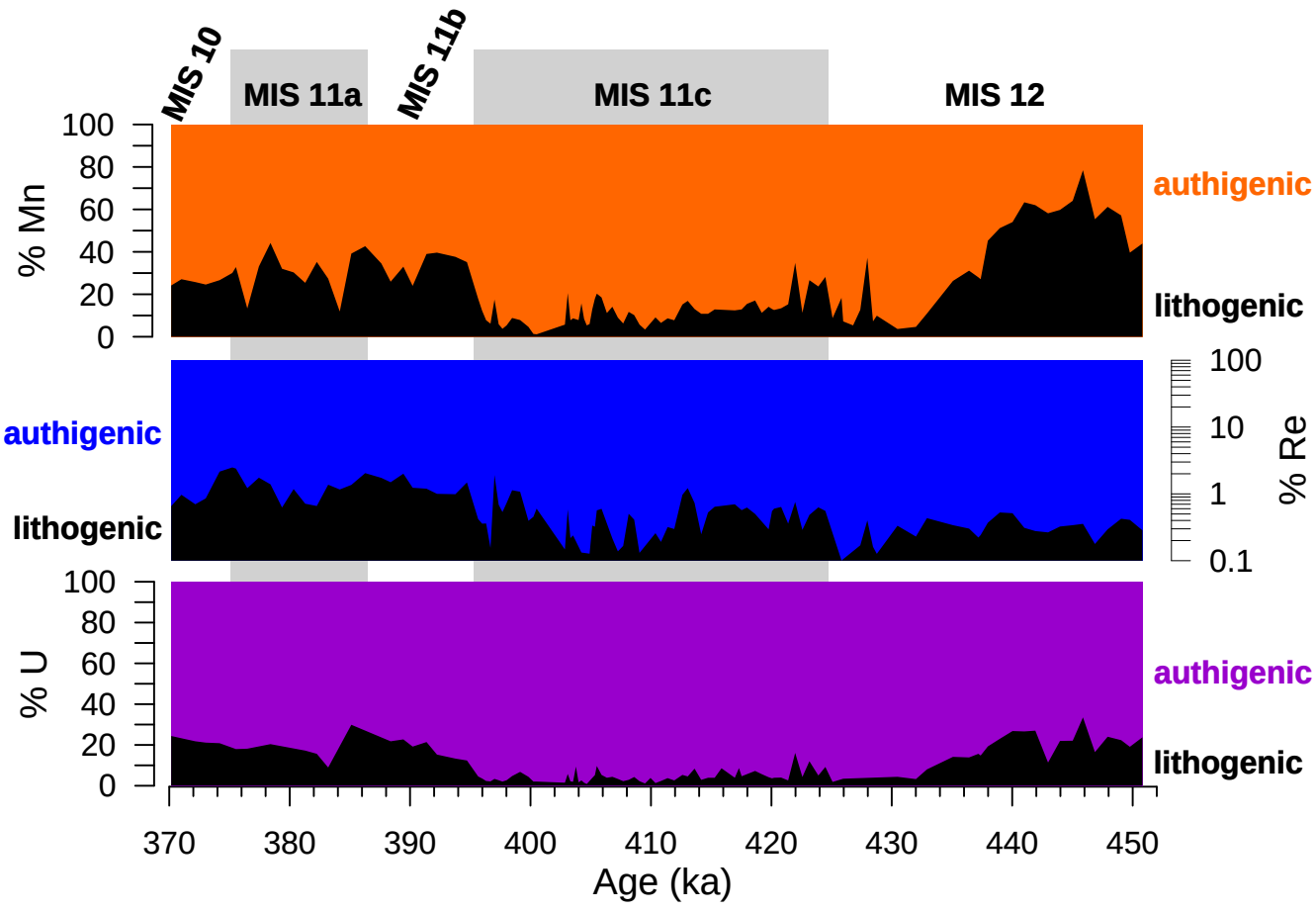
MIS 10
MIS 11a
MIS 11b
MIS 11c
MIS 12
% Mn
100
80
60
40
20
0
authigenic
lithogenic
authigenic
lithogenic
100
10
1
0.1
% Re
% U
100
80
60
40
20
0
authigenic
lithogenic
370
380
390
400
410
420
430
440
450
Age (ka)

Figure 5.

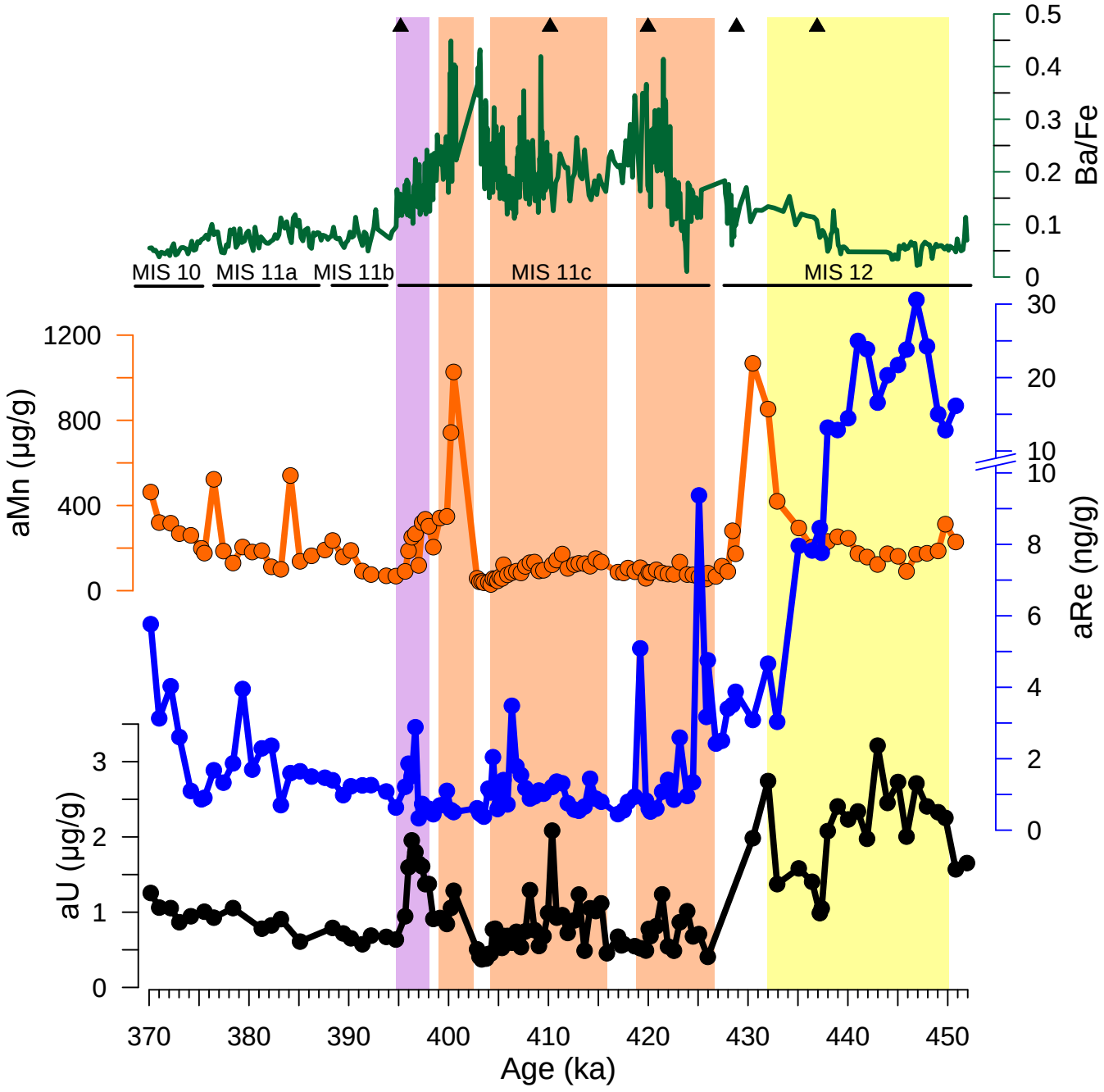
Ba/Fe
0.5
0.4
0.3
0.2
0.1
0
MIS 10
MIS 11a
MIS 11b
MIS 11c
MIS 12
aMn (µg/g)
1200
800
400
0
aRe (ng/g)
30
20
10
10
8
6
4
2
0
aU (µg/g)
3
2
1
0
370
380
390
400
410
420
430
440
450
Age (ka)

Figure 6.

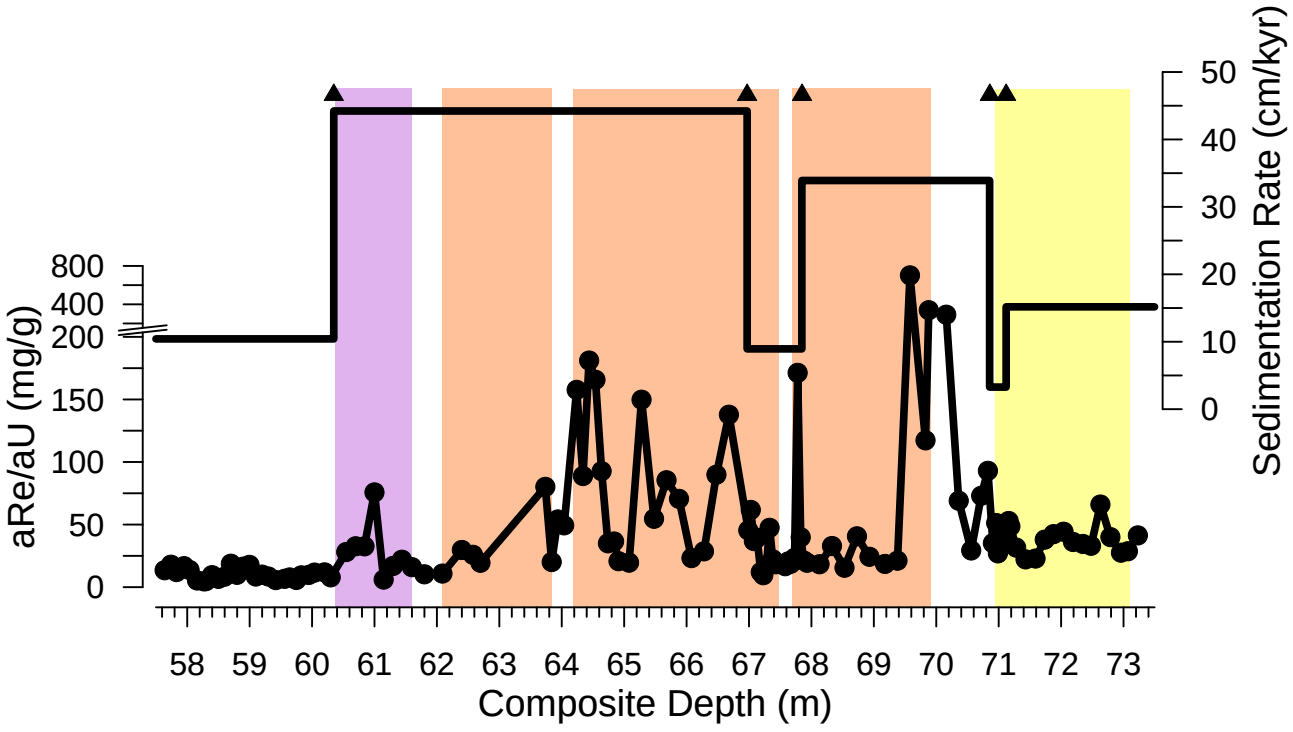
aRe/aU (mg/g)
800
400
200
150
100
50
0
Sedimentation Rate (cm/kyr)
50
40
30
20
10
0
58
59
60
61
62
63
64
65
66
67
68
69
70
71
72
73
Composite Depth (m)